Available online at www.sciencedirect.com
ScienceDirect
Journal of Solid State Chemistry 180 (2007) 1678–1685
JOURNAL OF SOLID STATE CHEMISTRY
www.elsevier.com/locate/jssc

# Systematic study of photoluminescence upon band gap excitation in perovskite-type titanates $R_{1/2}Na_{1/2}TiO_3$:Pr ($R$ = La, Gd, Lu, and Y)

Yoshiyuki Inaguma*, Takeshi Tsuchiya, Tetsuhiro Katsumata

*Department of Chemistry, Faculty of Science, Gakushuin University, 1-5-1 Mejiro, Toshima-ku, Tokyo 171-8588, Japan*

Received 14 December 2006; received in revised form 3 March 2007; accepted 15 March 2007
Available online 23 March 2007

**Abstract**

$Pr^{3+}$-doped perovskites $R_{1/2}Na_{1/2}TiO_3$:Pr ($R$ = La, Gd, Lu, and Y) were synthesized, and their structures, optical absorption and luminescent properties were investigated, and the relationship between structures and optical properties are discussed. Optical band gap of $R_{1/2}Na_{1/2}TiO_3$ increases in the order $R$ = La, Gd, Y, and Lu, which is primarily due to a decrease in band width accompanied by a decrease in Ti–O–Ti bond angle. Intense red emission assigned to *f–f* transition of $Pr^{3+}$ from the excited $^1D_2$ level to the ground $^3H_4$ state upon the band gap photo-excitation (UV) was observed for all compounds. The wavelength of emission peaks was red-shifted in the order $R$ = La, Gd, Y, and Lu, which originates from the increase in crystal field splitting of $Pr^{3+}$. This is attributed to the decrease in inter-atomic distances of Pr–O together with the inter-atomic distances ($R$, Na)-O, i.e., increase in covalency between Pr and O. The results indicate that the luminescent properties in $R_{1/2}Na_{1/2}TiO_3$:Pr are governed by the relative energy level between the ground and excited state of $4f^2$ for $Pr^{3+}$, and the conduction and valence band, which is primarily dependent on the structure, e.g., the tilt of $TiO_6$ octahedra and the Pr-Ti inter-atomic distance and the site symmetry of Pr ion.


*Keywords:* Luminescence; Praseodymium; Perovskite; Band gap; Titanate

## 1. Introduction

Energy transfer process is of much importance in photo-functional materials, and the novel materials presenting effective energy transfer and the elucidation of mechanism are strongly desired. Among them, much attention has been paid to metal oxides with the band gap energy corresponding to near ultraviolet or visible light, e.g. $TiO_2$ [1] and perovskite-type compounds such as $SrTiO_3$ [2,3] because of their potential use in photo-catalytic processes. Its promising applications include water splitting into $O_2$ and $H_2$, and the decomposition of harmful organic compounds in polluted air and water. Their photo-catalytic process depends upon the photo-excitation in accordance to band gap and successive energy transfer to split water into $H_2$ and $O_2$ or decompose organic compounds. Our research regarding photoluminescence in Pr-doped perovskites is related to the studies on photo-catalyst because both cases are common in the viewpoint of the usage of energy by band gap photo-excitation. Photoluminescence in most of rare-earth doped inorganic phosphor materials is attributed to the *f–f* transition or *f–d* transition of rare-earth ion as an activator and the intensity of photoluminescence depend on the site symmetry or sorts of ligands, i.e., the covalency between rare-earth ion and ligands. If the band gap photo-excitation process of phosphors and photoluminescence regarding *f*-transition of rare-earth ion are closely linked and the band excitation energy can be effectively converted, intense photoluminescence would be expected.

Diallio and Boutinaud et al. [4] have first found that Pr-doped perovskites $CaTiO_3$ shows intense red emission corresponding to *f–f* transition [5] of $Pr^{3+}$ from $^1D_2$ to $^3H_4$ on ultraviolet light excitation. After that, Cho et al. [6] reported the red cathodoluminescence properties. Then, Toki et al. [7] and Okamoto et al. [8–10] reported that $SrTiO_3$:$Pr^{3+}$ by the addition of Al exhibits an intense red

*Corresponding author. Fax: +81 3 5992 1029.
*E-mail address:* yoshiyuki.inaguma@gakushuin.ac.jp (Y. Inaguma).

0022-4596/$ - see front matter © 2007 Elsevier Inc. All rights reserved.
doi:10.1016/j.jssc.2007.03.017

emission approximately 200 times higher than for Al-free samples. Since their reports, $Pr^{3+}$-doped perovskite-type titanates $ATiO_3$ ($A$ = Ca [10–17], Sr [13,14,17,18], Ba [9,13,17,19,20], (La, Li) [21], $La_{1/2}Na_{1/2}$ [21], $La_{1/2}Ka_{1/2}$ [21]) have been attractive as red phosphor materials for a potential flat-panel display, field-emission display (FED). According to the previous reports [7–10,13], the red emission is attributed to the excitation from the valence band to the conduction band in host materials, and the energy transfer from the host to the activator $Pr^{3+}$. It was claimed that the energy transfer occurs from the host to the activator $Pr^{3+}$ through the recombination of photo-excited carriers in $ATiO_3$:$Pr^{3+}$ on the basis of the fact that the photoluminescence excitation spectra reveal the absorption edge of the $ATiO_3$ host lattice. It was then speculated that the overlapping between the absorption band of $ATiO_3$ host and the band for 4*f*–5*d* transition in $Pr^{3+}$ play an important role in the emission enhancement. Jia et al. [14] suggested that the energy transfer from $Pr^{3+}$ to the charge transfer state of the Ti-complex is related to the non-radiative transition, which is ascribed to the much weaker red emission in $SrTiO_3$:Pr than in $CaTiO_3$:Pr. Boutinaud et al. [15,16,22,23] proposed that the $Pr^{3+}/Ti^{4+} \leftrightarrow Pr^{4+}/Ti^{3+}$ inter-valence charge transfer state (IVCT) in Pr-doped titanates such as $CaTiO_3$:Pr is the final relaxation channel to the red emitting $^1D_2$ level. Kyomen et al. [17] then reported that the intense emission was observed when the IVCT band and the valence-to-conduction band edge are overlapped in $(Ca_{1-x}Sr_x)TiO_3$:Pr. The understanding with respect to the emission in Pr-doped titanates has become clearer owing to the previous studies. However, in order to elucidate the more detailed mechanism of photoluminescence, especially energy transfer process, further investigations are needed.

The entitled perovskite-type oxides $R_{1/2}Na_{1/2}TiO_3$:Pr ($R$ = La, Gd, Lu, and Y) are appropriate materials to elucidate the mechanism of photoluminescence systematically as well as potential red phosphors for the following reasons. Shan et al. [24–28] reported that $R_{1/2}Na_{1/2}TiO_3$ ($R$ = La, Pr, Nd, Gd, Eu, Tb, Yb, Y) have perovskite-type structure and the lattice parameter decreased and the tilting angle of $TiO_6$ octahedra increases with a decrease in the ionic radius [29] of $R$ ion. The change in lattice parameter and tilt angle of $TiO_6$ octahedron brings in the change in chemical bond between Ti and O, i.e., the change in width of valence and conduction bands which primarily consist of Ti 3*d* and O 2*p* orbitals [30]. Consequently, the change in band gap energy and energy transfer to $Pr^{3+}$ ion can be expected.

In this study, we investigated the structure, luminescent properties and their relationship of $R_{1/2}Na_{1/2}TiO_3$:Pr($R$ = La, Gd, Lu, and Y). Here we chose $La^{3+}$, $Gd^{3+}$, $Lu^{3+}$, and $Y^{3+}$ as $R$ ion because they exhibit no absorption of near ultraviolet and visible light due to the *f*–*f* transition. The mechanism of photoluminescence of Pr-doped perovskite titanates upon band gap photo-excitation is discussed.

## 2. Experimental

Perovskites $R_{1/2}Na_{1/2}TiO_3$ and $R_{1/2-x}Pr_xNa_{1/2}TiO_3$ ($x$ = 0.002) (abbreviated as $R$NTO and $R$NTO:Pr below, respectively) ($R$ = La, Gd, Lu, and Y) were synthesized by a conventional solid-state reaction at elevated temperature [26]. The starting materials were $La_2O_3$ (4N), $Gd_2O_3$ (4N), $Lu_2O_3$ (3N), $Y_2O_3$ (3N), $Na_2CO_3$ (3N), $Pr_6O_{11}$ (3N) and $TiO_2$ (3N). The metal contents of $La_2O_3$ and $Pr_6O_{11}$ were determined by a chelatometry with ethylenediaminetetraacetic acid (EDTA), and $R_2O_3$ ($R$ = Gd, and Lu) was fired at 1000 °C over a night prior to the weighing because the commercial reagents are non-stoichometric or include carbonates and hydroxides. The starting materials were mixed in their stoichiometric ratio with the addition of 2–5 mol% $Na_2CO_3$ powder, because $Na_2O$ has a tendency to vaporize at high temperature. The mixture of powders was pressed into a pellet and calcined at 1100 °C for 6 h in air. After grinding, the calcined powder was again pressed into pellets, sintered at 1250 °C for 4 h in air, and then furnace-cooled. $Na_2CO_3$ powder was added to the calcined powder in order to minimize impurity phases when they were observed. As reference compounds, $CaTiO_3$ and $SrTiO_3$ were also synthesized under the same heating condition by using the stoichometric mixture of $CaCO_3$ (3N) or $SrCO_3$ (3N) and $TiO_2$ (3N).

The phase identification and determination of lattice parameter for the sample were carried out by the powder X-ray diffraction method using a Rigaku RINT 2100 diffractometer (graphite-monochromatized Cu$K\alpha$). The crystal structures of $R$NTO ($R$ = La, Gd, Lu, and Y) were refined using the Rietveld method with the RIETAN 2000 program [31]. The X-ray diffraction data for Rietveld analysis were collected in the range $2\theta$ = 20–120° at 0.02° intervals at room temperature. The bond valence sum (BVS) was calculated from inter-atomic distances with the concept of bond valence [32,33].

The photoluminescence and excitation spectra measurements were carried out using a JASCO FP-6500 and 6600 spectrofluorometer at room temperature. Light from a 150 W xenon lamp was used as an excitation source. Photoluminescence spectra were recorded from 420 to 1010 nm with an excited wavelength of 345 and 440–460 nm, and excitation spectra were recorded from 250 to 550 nm with respect to the wavelength of luminescence peak. The emission and excitation spectra were corrected with the excitation spectrum of Rhodamine *B* in ethylene glycol (8 g/L) [34] and standard lamp. The diffuse reflectance spectra measurement was carried out using a JASCO V-550 ultraviolet and visible spectrophotometer.

## 3. Results and discussion

### 3.1. Crystal structure and optical band gap of RNTO ($R$ = La, Gd, Lu, and Y)

The powder X-ray diffraction experiments revealed that all the $R$NTO samples possess perovskite-type structure

(please see Figs. ES1–ES5 in Electronic Supplementary Information). A trace of impurity phases was observed only in LuNTO. The Pr-doped *R*NTO samples have the same structure as the pristine *R*NTO. The structure of LaNTO was refined with two different space groups, *I4/mcm* (No. 140) and $R\bar{3}$-*c* (No. 167) [35,36] since the axis of anti-phase tilt of $TiO_6$ was not discretely determined due to the low degree of lattice distortion. The Glazer notation [37,38] of tilt of $TiO_6$ is $a^0a^0c^-$ for *I4/mcm*, and is $a^-a^-a^-$ for $R\bar{3}$-*c*. In the former, the $TiO_6$ octahedron tilts along the tetragonal *c*-axis, resulting in the bond angles of Ti–O–Ti of 180° along tetragonal *c*-axis and less than 180° perpendicular to tetragonal *c*-axis. In the latter, the $TiO_6$ octahedron tilts along the hexagonal *c*-axis, resulting in one type of bond angle of Ti–O–Ti less than 180°. On the other hand, the structure of *R*NTO (*R* = Gd, Lu, and Y) was refined with the space group *Pnma* (No. 62) the same as the previous report [24,26]. The notation is $a^-b^+a^-$ for *Pnma,* as a result, there are two types of Ti–O–Ti bond whose angles are less than 180°. The results of Rietveld refinement are summarized in the Electronic Supplementary Information. The selected inter-atomic distances and angles of *R*NTO (*R* = La, Gd, Lu, and Y) were summarized in Table 1. The same as previous reports [24–28], the lattice parameters, *R*, Na–O distances, and Ti–O–Ti bond angles decrease; i.e., tilt angles increase, with increasing the ionic radius of *R* ion in *R*NTO (*R* = La, Gd, Lu, and Y). On the other hand, the Ti–O distances are similar despite of a decrease in the lattice parameters, resulting in the almost same BVSs of Ti (see Table 1). This means that the tilt of $TiO_6$ octahedron primarily compensates the decrease in the space of *A*-site ion.

The absorbance spectra of *R*NTO (*R* = La, Gd, Lu, and Y) at room temperature are shown in Fig. 1. Here, the diffuse reflectance data were transformed into absorbance with the Kubelka-Munk function. With a decrease in the ionic radius of *R*, the wavelength with respect to absorption edge decreases; i.e., the optical band gap energy, $E_g$, increases. Since the Ti–O inter-atomic distances are almost the same, the difference in $E_g$ cannot be explained by the difference in Ti–O inter-atomic distances. In $ATiO_3$, it is known that the orbital character of the valence band is primarily derived from Oxygen 2*p* orbitals, while the conduction band has strong Titanium 3*d* orbital character. Therefore, the chemical bond between Ti3*d* and O2*p* orbital become less covalent accompanied by the decrease of Ti–O–Ti bond angle and consequently the band width of bonding and anti-bonding orbitals decrease, resulting in the increase in band gap. Since the tilt angle of $TiO_6$ octahedron increases; i.e., Ti–O–Ti bond angle decreases with a decrease in the ionic radius of *R* for *R*NTO, the $E_g$ is expected to increase. Fig. 2 shows the variation of optical band gap energy, $E_g$, versus the average the Ti–O–Ti angles. As seen in Fig. 2, the $E_g$ of *R*NTO increases with decreasing the Ti–O–Ti bond angle. The result therefore implies that the $E_g$ of *R*NTO is primarily determined by the Ti–O–Ti angle. The data of $CaTiO_3$ and $SrTiO_3$ are then also plotted for reference. The estimated

Table 1
Selected inter-atomic distances (nm), bond angles (deg), and calculated bond valence sum (BVS) of Ti at room temperature for $R_{1/2}Na_{1/2}TiO_3$ (*R* = La, Gd, Lu, and Y)

| | $La_{1/2}Na_{1/2}TiO_3$ | | $Gd_{1/2}Na_{1/2}TiO_3$ | $Lu_{1/2}Na_{1/2}TiO_3$ | $Y_{1/2}Na_{1/2}TiO_3$ |
|---|---|---|---|---|---|
| | Model-1 (*I4/mcm*) | Model-2 (*R*3-*c*) | | | |
| *Distance* | | | | | |
| Ti–O1 | 0.19378(6) × 2 | 0.19494(4) × 6 | 0.1952(2) × 2 | 0.19551(12) × 2 | 0.19540(10) × 2 |
| Ti–O2 | 0.19540(9) × 4 | | 0.1932(7) × 2 | 0.1950(4) × 2 | 0.1951(3) × 2 |
| | | | 0.1965(7) × 2 | 0.1959(4) × 2 | 0.1966(3) × 2 |
| *R*, Na–O1 | 0.27406(6) × 4 | 0.2533(3) × 3 | 0.2353(10) × 1 | 0.2303(5) × 1 | 0.2329(4) × 1 |
| | | 0.27479(5) × 6 | 0.2523(6) × 1 | 0.2327(4) × 1 | 0.2405(3) × 1 |
| | | 0.2951(3) × 3 | 0.2980(7) × 1 | 0.3056(5) × 1 | 0.3055(4) × 1 |
| | | | 0.3047(10) × 1 | 0.3219(4) × 1 | 0.3121(3) × 1 |
| *R*, Na–O2 | 0.2570(4) × 4 | | 0.2397(6) × 2 | 0.2345(3) × 2 | 0.2350(2) × 2 |
| | 0.2923(5) × 4 | | 0.2571(8) × 2 | 0.2501(4) × 2 | 0.2557(3) × 2 |
| | | | 0.2720(8) × 2 | 0.2648(4) × 2 | 0.2666(3) × 2 |
| | | | 0.3193(6) × 2 | 0.3360(3) × 2 | 0.3310(2) × 2 |
| *R*, Na–Ti | 0.33565(6) × 8 | 0.33546(6) × 2 | 0.31826(14) × 2 | 0.30663(9) × 2 | 0.31197(10) × 2 |
| | | 0.33578(8) × 6 | 0.3270(2) × 2 | 0.32049(11) × 2 | 0.32414(13) × 2 |
| | | | 0.3338(2) × 2 | 0.33252(12) × 2 | 0.33320(13) × 2 |
| | | | 0.34658(15) × 2 | 0.35757(11) × 2 | 0.35301(12) × 2 |
| *Bond angle* | | | | | |
| Ti–O1–Ti | 180 | 167.69(15) | 156.7(5) | 151.77(17) | 154.2(2) |
| Ti–O2–Ti | 165.3(4) | | 157.4(3) | 151.7(2) | 153.12(13) |
| BVS of Ti | 4.18 | 4.17 | 4.17 | 4.09 | 4.09 |

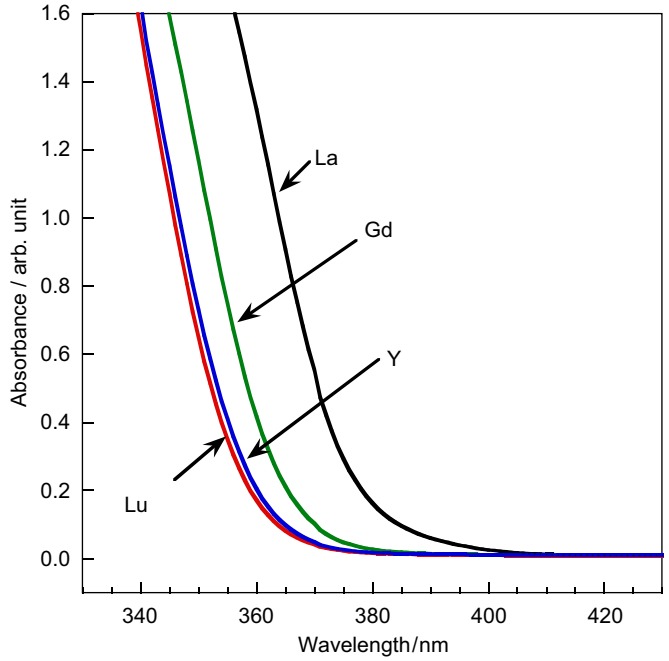


Fig. 1. The absorbance spectra of *R*NTO (*R* = La, Gd, Lu, and Y) at room temperature.

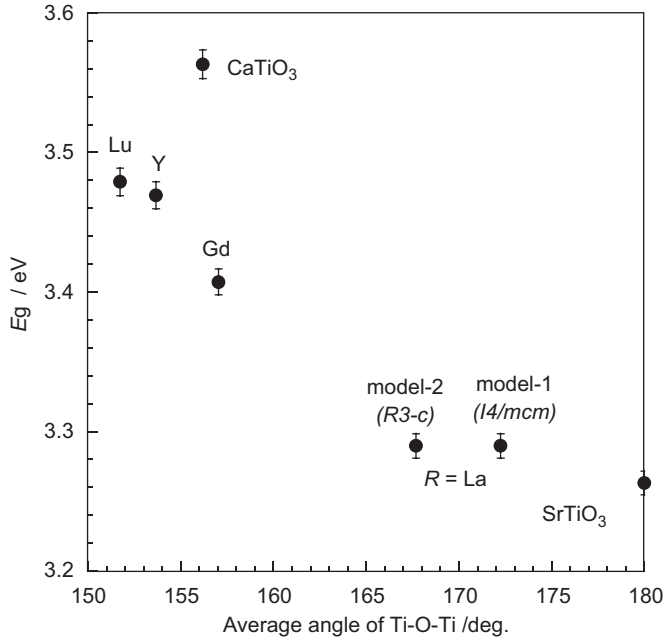


Fig. 2. Variation of optical band gap energy, $E_g$, versus average Ti–O–Ti angles of *R*NTO (*R* = La, Gd, Lu, and Y) at room temperature. The data of $CaTiO_3$ and $SrTiO_3$ are also plotted for reference.

band gap energies, 3.56 and 3.26 eV are in good agreement with those previously reported, 3.57 eV for $CaTiO_3$ [39] and 3.2 eV for $SrTiO_3$ [40], respectively. In Fig. 2, the structural data of $CaTiO_3$ after Sasaki et al. [41] is adopted. It seems that the data of $CaTiO_3$ and $SrTiO_3$ deviate from those of *R*NTO. This result implies that the band gap energies of $A^{2+}TiO_3$ and $R^{3+}_{1/2}Na^{+}_{1/2}TiO_3$ cannot be ruled only by the Ti–O–Ti angles derived from the average structure, and other factors, e.g., the local structure originated from the different *A*-site ions, $R^{3+}$ and $Na^{+}$, must be taken into account.

### 3.2. Optical absorption and luminescent properties of Pr-doped RNTO

The diffuse reflection spectra of *R*NTO:Pr (*R* = La, Gd, Lu, and Y) at room temperature are shown in Fig. 3. The absorption peaks in the vicinity of 400–500 and 610 nm were observed in addition to the absorption of band gap. These peaks correspond to the *f*–*f* transitions of $Pr^{3+}$ from $^3H_4$ to $^3P_2$(450–460 nm), $^3P_1$ and $^1I_6$(475–485 nm), $^3P_0$(490–500 nm), and $^1D_2$(610–620 nm) [5]. The shoulder band beside the absorption edge for *R*NTO:Pr (*R* = Gd, Lu, and Y) was then observed in the long wavelength side, and on the contrary the shoulder band was not observed in LaNTO:Pr. Fig. 4 shows the diffuse reflectance spectra of YNTO:Pr and YNTO. As seen in Fig. 4, the shoulder band was not observed in pristine YNTO, indicating that this band is related to Pr but is not an *f*–*f* transition of $Pr^{3+}$. Boutinaud et al. [15,16,22,23] found this type of absorption in Pr-doped $CaTiO_3$, and they proposed that this band is attributed to $Pr^{3+}/Ti^{4+} \leftrightarrow Pr^{4+}/Ti^{3+}$ IVCT as the final relaxation channel to the emitting $^1D_2$ level. They also pointed out [22,23] that the IVCT is dependent on the Pr–Ti shortest distance in Pr-doped $d^0$ transition-metal oxides and the IVCT can be observed when the distances are in the 0.315–0.330 nm. Supposing that Pr–Ti distance is approximately equal to *R*,Na–O inter-atomic distance, the shortest inter-atomic distances of Pr–Ti in *R*NTO:Pr

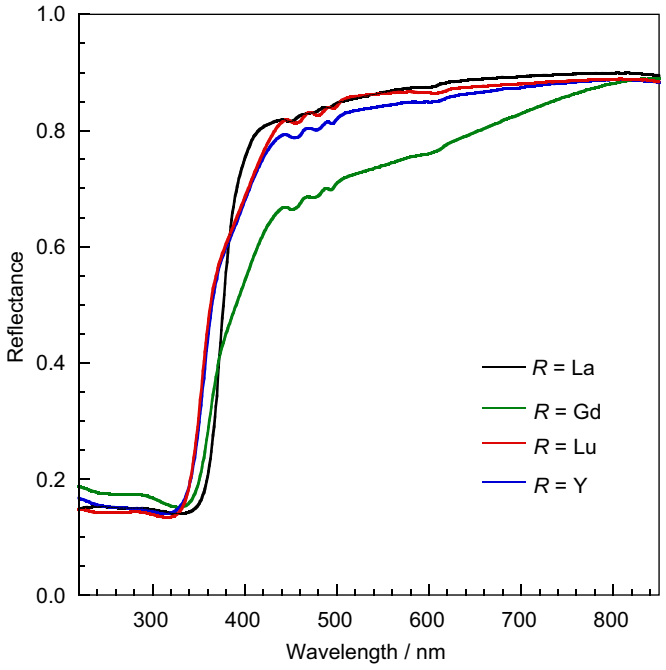


Fig. 3. Diffuse reflectance spectra of $R_{1/2}Na_{1/2}TiO_3$:Pr 0.2% (*R* = La, Gd, Lu, and Y).

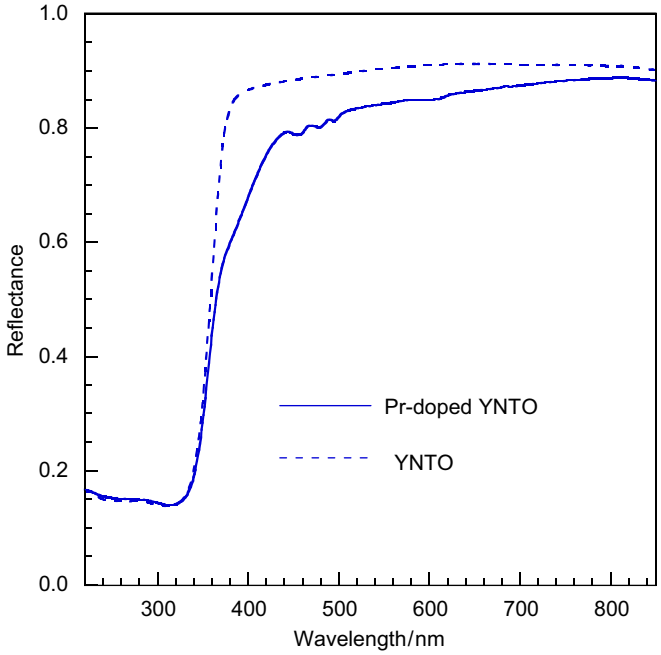


Fig. 4. Diffuse reflectance spectra of $Y_{1/2}Na_{1/2}TiO_3$:Pr (solid line) and $Y_{1/2}Na_{1/2}TiO_3$ (dashed line).

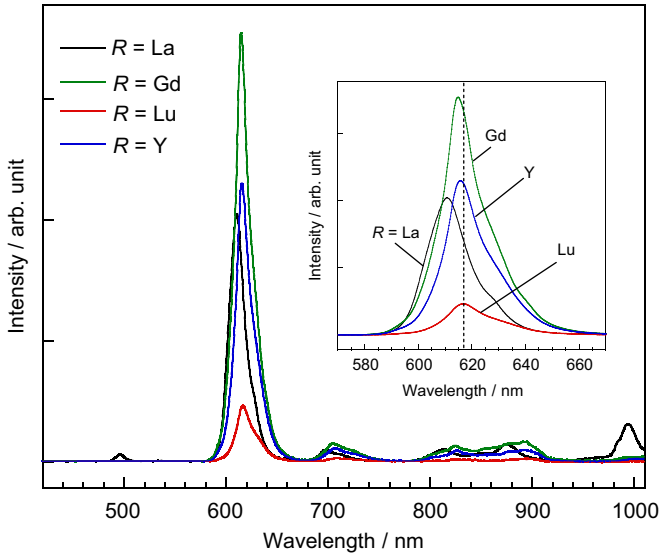


Fig. 5. Emission spectra of $R_{1/2}Na_{1/2}TiO_3$:Pr 0.2 mol% ($R$ = La, Gd, Lu, and Y) under an excitation at 345 nm. Inset shows the profiles of red $^1D_2$ emission.

($R$ = La, Gd, Lu, and Y) are 0.336, 0.318, 0.307, and 0.312 nm seen in Table 1, respectively. The obtained result is therefore in good agreement with the findings by Boutinaud et al. In addition, they stated that the IVCT is present at a higher energy level and overlaps the absorption of host materials even when the inter-atomic distance of Pr-Ti is beyond 0.330 nm. This idea can explain no absorption corresponding to the IVCT in LaNTO:Pr. As another possibility, the finding is also likely to be ascribed to poor energy transfer from 4*f* orbital of Pr to 3*d* orbital of Ti due to the long inter-atomic distance of Pr–Ti despite that the energy difference between Pr 4*f* and Ti 3*d* being the same as *R*NTO:Pr ($R$ = Gd, Lu and Y).

Fig. 5 shows the emission spectra of *R*NTO:Pr ($R$ = La, Gd, Lu, and Y) under an excitation at 345 nm. All the compounds show intense red emission with a wavelength, $\lambda$, of 610–616 nm, corresponding to the *f*–*f* transition of $Pr^{3+}$ ($^1D_2$ to $^3H_4$), and several emissions in near infrared-red region, corresponding to the transitions of $^1D_2$ to $^3H_5$ ($\lambda$~700 nm), $^1D_2$ to $^3H_6$ ($\lambda$~820 nm), $^1D_2$ to $^3F_2$ ($\lambda$~880 nm) and $^1D_2$ to $^3F_3$, $^3F_4$ ($\lambda$~1000 nm) [5]. As seen in the inset of Fig. 5, the wavelength of red emission peaks was red-shifted in the order $R$ = La, Gd, Y, and Lu. Other peaks in the infrared-red region were red-shifted in the same way. Furthermore, the absorption peaks corresponding to the *f*–*f* transitions of $Pr^{3+}$ from $^3H_4$ to $^3P_2$, $^1I_6$ and $^3P_1$, $^3P_0$, and $^1D_2$ is seen in Fig. 4, also show the same tendency. These findings originate from the increase in the crystal field spilitting due to the increase in covalency between Pr and oxygen, i.e., the decrease in inter-atomic distance of Pr–O in *R*NTO:Pr. As seen in Table 1, the inter-atomic distance of ($R$, Na)–O decreases in the order $R$ = La, Gd, Y, and Lu. These results indicate that the inter-atomic distance of Pr–O in *R*NTO:Pr also decreases together with a decrease in inter-atomic distance of ($R$, Na)–O, resulting in the increase in covalency between Pr and oxygen. The weak green-blue emission corresponding to the *f*–*f* transition of $^3P_0$ to $^3H_4$ was then observed in LaNTO though the green-blue emission in other compounds was little observed. This phenomenon will be discussed later.

Fig. 6 shows the emission and excitation spectra of *R*NTO:Pr ($R$ = La, Gd, Lu, and Y). Here the excitation spectra were recorded with respect to the red luminescence peak. Compared with Figs. 4 and 6, the peak of excitation is in agreement with the optical absorption edge. This finding indicates that the red intense luminescence is mainly based upon the band-gap photo-excitation of *R*NTO:Pr. The shoulders adjacent to absorption edge seen in diffuse reflectance spectra of *R*NTO ($R$ = Gd, Lu, and Y), also corresponds to the shoulder of excitation spectra. The IVCT pointed out by Boutinaud et al. [15,16,22,23], is therefore one of the pathway of energy transfer for red emission in *R*NTO:Pr ($R$ = Gd, Lu, and Y).

On the other hand, upon photo-excitation to the excited states of $Pr^{3+}$, $^3P_2$, $^3P_1$, and $^3P_0$, poor red emission was observed. Fig. 7(a) and (b) show the luminescence spectra upon band gap excitation ($\lambda$ = 345 nm) and the excitation in accordance to *f*–*f* transition ($^3H_4$ to $^3P_2$, $\lambda$ = 455 nm) of *R*NTO:Pr ($R$ = La and Y), respectively. The red emission upon band gap excitation is much more intense relative to that upon the *f*–*f* excitation of $^3H_4$ to $^3P_2$ for both compounds, indicating the effective energy transfer of band gap excitation energy. The calculated peak intensity ratio of green-blue emission (~490 nm) to red emission (~610 nm) (G/R ratio) upon band gap excitation and upon $^3H_4$ to $^3P_2$ excitation using the spectrum data shown

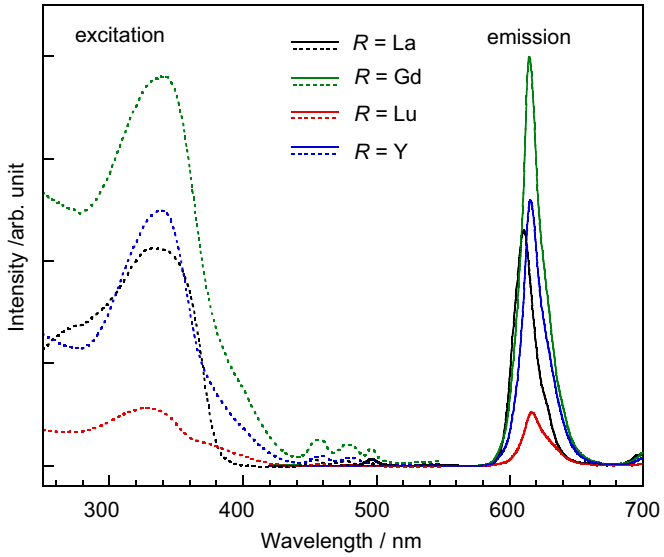


Fig. 6. Emission (excitation: 345 nm) and excitation (emission: 610–616 nm) spectra of $R_{1/2}Na_{1/2}TiO_3$:Pr 0.2 mol% ($R$ = La, Gd, Lu, and Y).

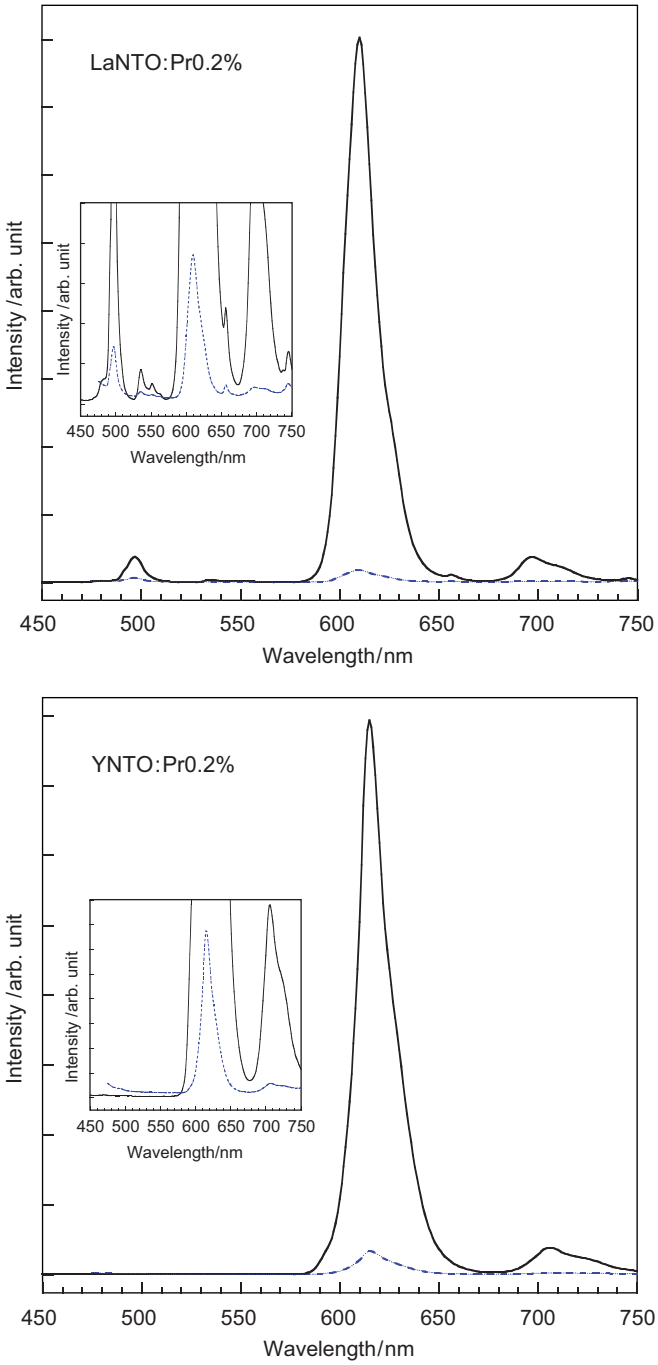


Fig. 7. Emission spectra upon photo-excitation of 345 nm (solid line) and of 455 nm(dashed line) for $R_{1/2}Na_{1/2}TiO_3$:Pr 0.2 mol% ($R$ = La and Y). The enlarged figures are shown in the insets.

in Fig. 7 are 5% and 40% for LaNTO:Pr, and <0.1% and 6% for YNTO:Pr, respectively. These results imply that the red emission occurs via the different route upon two different excitations. Upon the photo-excitation from $^3H_4$ to $^3P_2$, the route is simply from the $^3P_0$ excite state to the $^3H_4$ ground state. On the other hand, upon band gap excitation, the main relaxation channel is not that via $^3P_0$ excite state, but the channel from the conduction band via an excited state $^1D_2$ of $Pr^{3+}$ to finally $^3H_4$ ground state. Furthermore, the evident differences in G/R ratio between LaNTO:Pr and YNTO:Pr were also found. Upon photo-excitation from $^3H_4$ to $^3P_2$, the difference between two compounds (G/R ratio: 40% and 6%) is partly ascribed to the difference in transition probability due to the difference of site symmetry of Pr between LaNTO (space group: $I4/mcm$ or $R\bar{3}$-$c$, point group: $\bar{4}2m$ or 32) and YNTO (space group: $Pnma$, point group: $m$). Upon band gap excitation, the weak green-blue emission was observed for LaNTO:Pr, on the contrary, the emission for $R$NTO:Pr ($R$ = Gd, Lu, and Y) was almost quenched as mentioned before. The large difference in R/B ratio (5% and <0.1%) cannot be explained only by the difference in site symmetry. Boutinaud et al. [15,16,22,23] claimed that the quenching of green-blue emission from $^3P_0$ upon band gap excitation is related to the energy level of IVCT relative to the energy level of conduction band. Their idea can be applied to account for our results. Considering another possibility, it is likely that a part of Pr ions are accommodated in Ti-site in LaNTO and the green-blue emission originates from the Pr ion in Ti-site. We therefore also need to elucidate the relationship between the site preference of Pr and the luminescent properties.

The obtained results indicates that the intense red emission in $R$NTO:Pr is based on the two different routes. One is due to the IVCT via oxygen, $Pr^{3+}/O^{2-}/Ti^{4+} \leftrightarrow Pr^{4+}/O^{2-}/Ti^{3+}$ proposed by Boutinaud et al. [15,16,22,23]. The electron of $Pr^{3+}$ is excited to the IVCT state and here charge transfer to $Ti^{4+}$ occurs via O 2$p$ orbital, and then the electron returns to the Pr ion in the excited state, $^1D_2$ [42]. Finally the transition accompanied by red emission to the ground state, $^3H_4$, occurs. Another one is upon band gap excitation. The schematic diagram of the band gap excitation and emission processes is shown in Fig. 8. The electron in the valence band which primarily consists of O 2$p$ orbital is photo-excited into the

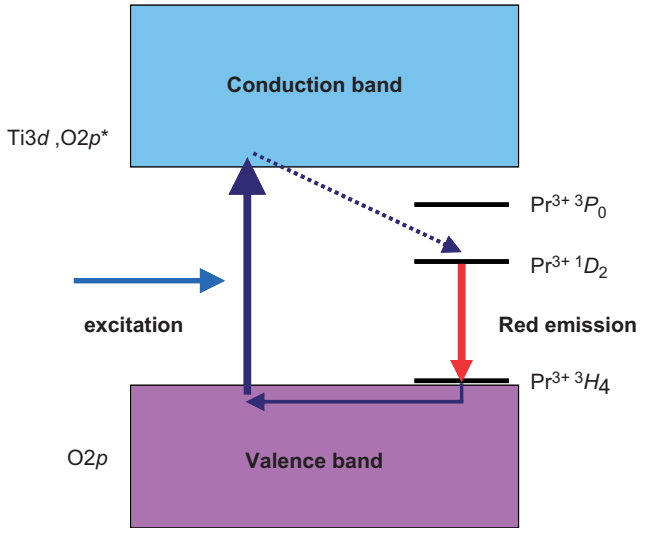


Fig. 8. Schematic diagram of the band-gap excitation and emission processes in $R_{1/2}Na_{1/2}TiO_3$:Pr.

conduction band which primarily consists of Ti 3*d* and O 2*p* orbitals, and then the electron of $Pr^{3+}$ is transferred to the O 2*p* orbital in the valence band i.e., the generated hole accompanied by the excitation of electron is transferred to the $Pr^{3+}$. The excited electron in conduction band relaxes to the excited state of $Pr^{3+}$, $^1D_2$ (this relaxation process may be via the IVCT state), and then returns to the ground state of $Pr^{3+}$, which is accompanied by the red emission. The formal charge transfer in these processes is described as follows:

$$O^{2-} + Pr^{3+} \rightarrow O^{-}(= O^{2-} + h^{+}) + Pr^{3+} + e^{-} \rightarrow$$
$$O^{2-} + Pr^{4+} + e^{-} \rightarrow O^{2-} + Pr^{3+*} \rightarrow O^{2-} + Pr^{3+}$$

Here, "$Pr^{3+}$*" denotes the $Pr^{3+}$ ion which is in the excited state.

The electron transfers from the conduction band to the excited state of $Pr^{3+}$, $^1D_2$, and from the ground state of $Pr^{3+}$, $^3H_4$ to the valence band, are dependent on the relative level of ground and excited state of $4f^2$ for $Pr^{3+}$ to the level of conduction and valence band. Therefore, the structural features, i.e., the tilt of $TiO_6$ octahedra and Pr–Ti inter-atomic distance which determine the electronic structure and the energy levels of host lattice and $Pr^{3+}$ ion, are predominant factors of intense red emission in *R*NTO:Pr, bringing in the systematic differences in luminescent properties between *R*NTO:Pr ($R$ = La, Gd, Lu, and Y). The further knowledge of the precise energy level for the ground and excited state of $4f^2$ for $Pr^{3+}$, and the conduction and valence band would elucidate the emission mechanism in more detail.

## 4. Conclusions

It was found that the effective energy transfer of band gap excitation energy to emission process occurs in $R_{1/2}Na_{1/2}TiO_3$:Pr ($R$ = La, Gd, Lu, and Y), resulting in the intense red emission assigned to *f*–*f* transition from the excited $^1D_2$ level to the ground $^3H_4$ state of $Pr^{3+}$. The tilt of $TiO_6$ octahedra changes the band width, bringing in the increase in the optical band gap of $R_{1/2}Na_{1/2}TiO_3$ in the order $R$ = La, Gd, Y, and Lu. The red-shift in emission peaks in the order $R$ = La, Gd, Y, and Lu reveals that the inter-atomic distance between Pr and O decreases with a decrease in (*R*, Na)–O average distance. The differences in luminescent properties for $R_{1/2}Na_{1/2}TiO_3$:Pr are ruled by the relative energy level between the ground and excited state of $4f^2$ for $Pr^{3+}$, and the conduction and valence band, which is strongly correlated to the structure, e.g., the tilt of $TiO_6$ octahedra and the Pr-Ti inter-atomic distance and the site symmetry of Pr ion.

## Acknowledgments

The authors are grateful to the reviewers for their useful advice and comments. This work was supported by a Grant-in-Aid for Scientific Research (c) (No. 17560598) of Japan Society for the Promotion of Science, the Grant-in-Aid for Scientific Research on Priority Area, "Nanoionics (439)", and "High-Technology Research Center Project", of the Ministry of Education, Culture, Sports, Science and Technology of Japan.

## Appendix A. Supplementary materials

Supplementary data associated with this article can be found in the online version at doi:10.1016/j.jssc.2007.03.017.

## References

[1] A. Fujishima, K. Honda, Nature (London) 238 (1972) 37.
[2] M.S. Wrighton, A.B. Ellis, P.T. Wolczanski, D.L. Morse, H.B. Abrahamson, D.S. Ginley, J. Am. Chem. Soc. 98 (1976) 2774.
[3] K. Domen, A. Kudo, T. Onishi, J. Catal. 102 (1986) 92.
[4] P.T. Diallo, P. Boutinaud, R. Mahiou, J.C. Cousseins, Phys. Status Solidi A 160 (1997) 255.
[5] G.H. Dieke, H.M. Crosswhite, Appl. Opt. 2 (1963) 675.
[6] S.H. Cho, J.S. Yoo, J.D. Lee, J. Electrochem. Soc. 143 (1996) L231.
[7] H. Toki, Y. Sato, K. Tamura, S. Itoh, Proceedings of the Third International Display Workshop, Kobe, Japan, vol. 2, 1996, pp. 519–520;
S. Itoh, H. Toki, K. Tamura, F. Kataoka, Jpn. J. Appl. Phys. 38 (1999) 6387.
[8] S. Okamoto, H. Kobayashi, H. Yamamoto, J. Appl. Phys. 86 (1998) 5594.
[9] H. Yamamoto, S. Okamoto, Display 21 (2001) 93.
[10] S. Okamoto, H. Yamamoto, Appl. Phys. Lett. 78 (2001) 655.
[11] P.T. Diallo, K. Jeanlouis, P. Boutinaud, R. Mahiou, J.C. Cousseins, J. Alloy. Compds. 323–324 (2001) 218.
[12] Y. Pan, Q. Su, H. Xu, T. Chen, W. Ge, C. Yang, M. Wu, J. Solid State Chem. 174 (2003) 69.
[13] S. Okamoto, H. Yamamoto, J. Lumin. 102–103 (2003) 586.
[14] W. Jia, W. Xu, I. Rivera, A. Perez, F. Fernandez, Solid State Commun. 126 (2003) 153.
[15] E. Pinel, P. Boutinaud, R. Mahiou, J. Alloy Compds. 380 (2004) 225.

[16] P. Boutinaud, E. Pinel, M. Dubois, A.P. Vink, R. Mahiou, J. Lumin. 111 (2005) 69.
[17] T. Kyômen, R. Sakamoto, N. Sakamoto, S. Kunugi, M. Itoh, Chem. Mater. 17 (2005) 3200.
[18] H. Yamamoto, S. Okamoto, H. Kobayashi, J. Lumin. 100 (2002) 325.
[19] S. Okamoto, H. Yamamoto, J. Appl. Phys. 91 (2002) 5492.
[20] J. Li, Y.-J. Wu, M. Kuwahara, Jpn. J. Appl. Phys. 44 (2005) L708.
[21] K.A. Hyeon, S.H. Byeon, J.C. Park, D.K. Kim, K.S. Suh, Solid State Commun. 115 (2000) 99.
[22] P. Boutinaud, E. Pinel, M. Oubaha, R. Mahiou. E. Cavalli, M. Bettinelli, Opt. Mater. 28 (2006) 9.
[23] P. Boutinaud, R. Mahiou, E. Cavalli, M. Bettinelli, Chem. Phys. Lett. 418 (2006) 185.
[24] P.-H. Sun, T. Nakamura, Y.-J. Shan, Y. Inaguma, M. Itoh, Ferroelectrics 200 (1997) 93.
[25] T. Nakamura, Y.-J. Shan, P.-H. Sun, Y. Inaguma, M. Itoh, Solid State Ion. 108 (1998) 53.
[26] Y.-J. Shan, T. Nakamura, Y. Inaguma, M. Itoh, Solid State Ion. 108 (1998) 123.
[27] Y.-J. Shan, T. Nakamura, P.-H. Sun, Y. Inaguma, M. Itoh, Ferroelectrics 218 (1998) 161.
[28] T. Nakamura, Y.-J. Shan, M. Miyata, K. Kobashi, Y. Inaguma, M. Itoh, Korean J. Ceram. 5 (1999) 82.
[29] R.D. Shannon, Acta Crystallogr. A 32 (1976) 751.
[30] H.W. Eng, P.W. Barnes, B.M. Auer, P.M. Woodward, J. Solid State Chem. 175 (2003) 94.
[31] F. Izumi, T. Ikeda, Mater. Sci. Forum 321–324 (2000) 198.
[32] D. Altermatt, I.D. Brown, Acta Crystallogr. B 41 (1985) 240; I.D. Brown, D. Altermatt, Acta Crystallogr. B 41 (1985) 244.
[33] N.E. Brese, M. O'Keeffe, Acta Crystallogr. B 47 (1985) 192.
[34] W.H. Melhuish, J. Opt. Soc. Am. 52 (1962) 1256.
[35] R.H. Mitchell, A.R. Chakmouradian, P.M. Woodward, Phys. Chem. Miner. 27 (2000) 583.
[36] R. Ranjan, A. Senyshyn, H. Boysen, C. Baehtz, F. Frey, J. Solid State Chem. 180 (2007) 995.
[37] M. Glazer, Acta Crystallogr. B 28 (1972) 3384.
[38] M. Glazer, Acta Crystallogr. A 31 (1975) 756.
[39] K. Ueda, H. Yanagi, R. Noshiro, H. Hosono, H. Kawazoe, J. Phys.: Condens. Matter 10 (1998) 3669.
[40] M. Cardona, Phys. Rev. 140 (1965) A651.
[41] S. Sasaki, C.T. Prewitt, J.D. Bass, W.A. Schulze, Acta Crystallogr. C 43 (1987) 1668.
[42] E.G. Reut, A.L. Ryskin, Phys. Status Solidi A 17 (1973) 47.